IOP Publishing Journal Title
Flex. Print. Electron. (XXXX) XXXXXX https://doi.org/XXXX/XXXX

Reliability test of fully printed and flexible organic electrolyte-based supercapacitor

Chakra Rokaya[1], Jari Keskinen[1], Sanna Lahokallio[2] and Donald Lupo[1]

[1] Faculty of Information Technology and Communication Sciences, Tampere University, Korkeakoulunkatu 3, 33720 Tampere, Finland
[2] Trelic Oy, Tekniikankatu 1, FI-33720 Tampere, Finland

E-mail: Chakra.Rokaya@tuni.fi

Received xxxxxx
Accepted for publication xxxxxx
Published xxxxxx

Abstract

As the demand for supercapacitors in various flexible and wearable energy sectors grows, reliability becomes a key aspect to consider. We report the fabrication and reliability study of printed, flexible organic electrolyte-based supercapacitors. The supercapacitor can be operated over a wide temperature range from -40 °C to 100 °C with excellent repeatability and stability. Thermal shock tests led to a defect in the electrode layer's microstructure, which reduces the supercapacitor performance. Cyclic bending experiments show that the device has excellent robustness, mechanical flexibility, long-term electrical stability, and 100 % capacitance retention up to 10000 bending cycles with a bending radius of 0.41 cm. Thus, the device is suitable for wearable and flexible energy storage applications over a wide temperature range.

Keywords: Supercapacitor, Reliability, Electrolyte, Flexible, Temperature

1. Introduction

With the recent growth in portable, flexible, wearable, miniaturized electronic products, the demand for flexible and reliable energy storage devices such as supercapacitors has increased. An energy storage device for such applications should be low-cost, environmentally friendly, lightweight, and operate over a wide temperature range [1]. Supercapacitors offer a solution to meet the growing demand for consumer electronics.

Supercapacitors, also known as electric double-layer capacitors (EDLC), ultracapacitors, or electrochemical capacitors [2][3]. Supercapacitors have attracted great attention because of their high efficiency, long cycle life, high power densities, wide temperature ranges [4][5], and quick charging time [6]. In many energy applications, supercapacitors are used for providing short term power peaks to devices such as electric vehicles and power tools, as well as for storing energy to power active RFID tags, sensors, sensor networks, and Internet of Things devices (IoT) when the primary energy source is unavailable [7]. Supercapacitors can also be suitable for operation over temperatures from -40 °C to 100 °C [8][9]. Maintaining the power density, thermal stability, cyclic stability, and electrical performance without significant loss over a wide range of temperatures is a very important advantage of supercapacitors for many applications, such as portable electronic devices, aerospace power sources for actuator systems, charging stations for electric vehicles, military weapons and armored vehicles [8][10]. In general, a supercapacitor is made up of highly porous electrodes, current collectors, separator, and electrolyte. The operation voltage of supercapacitors is limited due to the electrochemical window of the electrolyte. Compared to the aqueous electrolyte, organic electrolytes can have higher potential window. Some organic electrolytes can provide potential up to 3.3 V, where as with aqueous electrolyte the maximum potential is about

1.3 V [11][12]. In this reliability study, we used supercapacitors comprising propylene carbonate electrolyte, which can provide up to 2.5 V per cell despite being of low toxicity and cost.

Reliability is a method to check whether the device can perform a required task in specific condition for a given time interval, and has been applied to supercapacitors as well [13][14]. Reliability testing, including the determination of failure mechanisms [15], is very important, due to energy storage demand at extreme conditions, and is widely applied to power electronics systems and devices such as inductors, semiconductors, inverters, capacitor banks [16][17] *etc*., as well as to supercapacitors. Kötz *et al* [9] investigated temperature dependency behavior of an activated carbon (AC)-based supercapacitor in the range -40 °C to 70 °C using 1 M tetraethyl ammonium tetrafluoroborate ($TEABF_4$) in acetonitrile and in propylene carbonate (PC). Similar temperature dependent measurement was reported by Liu *et al* [18] and Gualous *et al* [19]. In those cases, the temperature was limited to below 80 °C, even though PC electrolytes can withstand higher temperatures [20]. Azais *et al* [21] investigated electrode pore blockage and gas evolution due to organic electrolyte decomposition on electrode materials. Bitter *et al* [22] observed structural modification of the electrode because of oxidation and reduction. Hahn *et al* [23] found that overvoltage led to a significant expansion of the electrode, and even nominal voltage might result in decomposition of electrode and electrolyte. Oz *et al* [24] investigated the microstructure of the electrode-electrolyte interface changes upon degradation and electrolyte parasitic reactions resulting in precipitation onto the porous surface. This limits the transport of the electrolyte ions to the porous electrode and reduces the performance. Lu *et al* reported thermally stable montmorillonite/poly(vinyl alcohol) (MMT/PVA) hydrogen gel electrolyte based supercapacitors operating at temperature ranges -50 °C to 90 °C and the study on mechanical deformation of the devices for flexible energy storage application [25]. Dai *et al* review on development, progress, and mechanical properties of different types of gel electrolytes based flexible supercapacitors. The author mentioned that the polymer gel electrolyte has self healing properties and several advantages in terms of cyclic stability, safety, flexibility, and wide temperature range [26]. Sundriyal *et al* reported optimized electrode patterned-inkjet printed planar micro supercapacitors, which were flexible and cyclic stability up to 20000 cycles [27]. Liu *et al* reported a anti-freezing polymer hydrogel electrolyte based supercapacitors operating at temperature range -20 to 100 °C with capacitance retention about 90 % [28]. Na *et al* studied the electrochemical performance and mechanical reliability of supercapacitors made with heterogeneous hybrid composite fibers consists of carbon nanotube yarn (CNTY) and metal organic frameworks (MOFs) [29]. However, so far the thermal and mechanical reliability of flexible, printed supercapacitors based on PC electrolyte has not been systematically studied and reported.

Under extreme conditions, storing energy is still very challenging. A key goal of reliability testing of supercapacitors is to determine their ability to reliably fulfill performance requirements over the targeted range of operating conditions. We have previously reported similar devices as energy storage units for low power electronics [30]. Here, we report the results of systematic reliability studies on these devices in different environments, concentrating on performance over a range of temperatures, cyclic bending stability, and reaction to thermal shock. We confirm the functionality of these devices, and possible reasons for the failure following thermal shock tests. In addition, further necessary steps to overcome those failures and design optimization to meet requirements for performance are discussed.

2. Experiments

The schematic structure of the supercapacitor is shown in figure **1(**a,b**)**. We have reported the fabrication process of similar supercapacitors earlier and briefly summarize the process here [2][30][31][32]. A polyethylene terephthalate and aluminum (5 cm by 4.5 cm) (PET/Al, Pyroll, thicknesses 50 µm and 9 µm, respectively) was used as a current collector. The electrode ink was made with 90 wt% of highly conductive Super P carbon (Timcal) and 10 wt% carboxymethyl cellulose (CMC) binder. The deionized water added to the mixture to suitable viscosity. The target use case for these devices is as a power peak provider for Bluetooth Low Energy (BLE) transmission in conjunction with a small, printed battery; as a result, the target was a relatively small capacitance of a few mF and a low ESR on the order of 1-2 Ohm. We therefore formulated an electrode ink based on super P carbon black which yields lower capacitance than activated carbon, and also reduces ESR due to high conductivity. These supercapacitors can store sufficient energy and deliver sufficient peak power for a BLE transmission [30]. The laboratory-scale coating unit (Mtv Messtechnik), shown in figure **1**(c), was used for stencil printing of the electrodes on the current collector (substrate). The electrode area of the fabricated supercapacitor was 2 cm by 3 cm and the wet thickness of the was 100 µm. The curing temperature of electrodes were 60 °C for 15 minutes.

Once curing was completed, the electrodes were moved to a nitrogen-filled glove box in order to assemble the device in a clean environment free of water and oxygen. Then, 1 M tetraethylammonium tetrafluoroborate ($TEABF_4$) in propylene carbonate (PC) electrolyte was prepared. Although there are other organic electrolytes with wider electrochemical windows (the maximum voltage per cell in the reported devices are 2.5 V), PC was chosen due to low cost and low

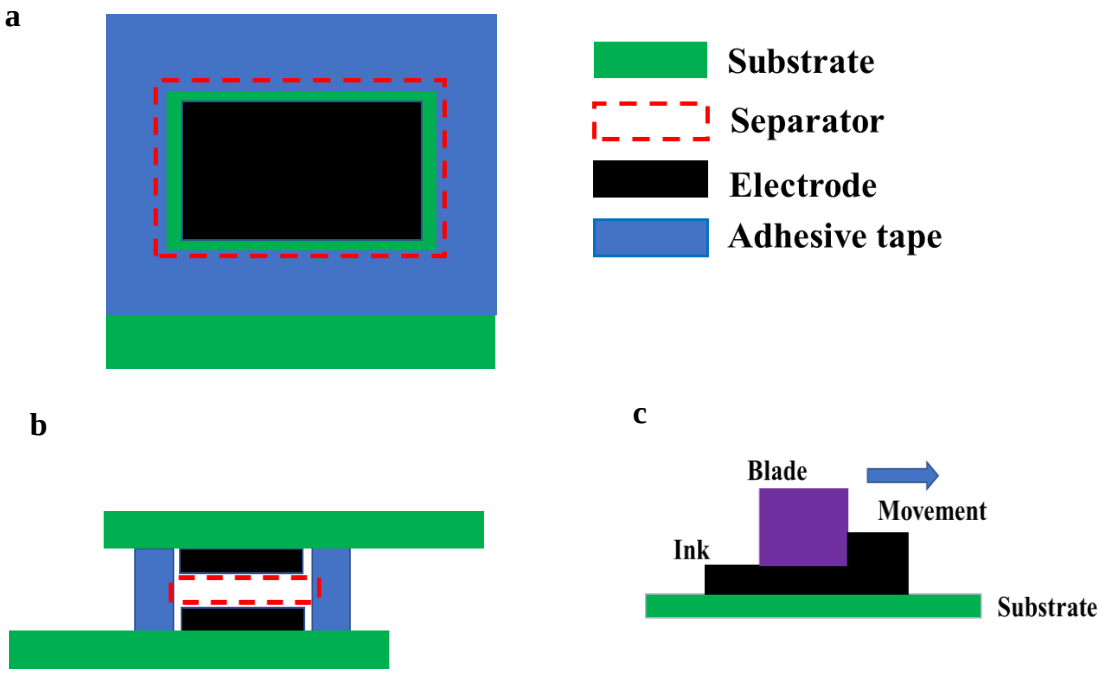

Figure 1. Schematic drawing of electrode top view(a), a cross-section of the entire device (b), and stencil printing method (**c**). Layer thickness is not to scale

toxicity. Before assembling the device, the separator and electrode surface was made wet enough with electrolyte, so that the pores get filled. The supercapacitors were then assembled in a sandwiched structure. The electrodes were aligned face to face, separated by the separator (Dreamweaver Titanium 40, dimension 2.5 cm by 3.5 cm). The 3M adhesive tape was used for the adhesion of the electrodes. The overall thickness of the device was about 0.5 mm.

A Zennium electrochemical workstation (Zahner Elektrik GmbH) and software were used for cyclic voltammetry (CV) and electrochemical impedance spectroscopy (EIS) measurements. The supercapacitors were characterized before and after testing. From these, the capacitance and equivalent series resistance (ESR) were determined. Based on the reliability analysis from the cyclic voltammetry at different scan rates and electrochemical impedance spectroscopy, the variation of the capacitance and equivalent series resistance was explained.

Initially, device performance over a wide temperature window ranging from -40 °C to 100 °C was studied. Electrolyte conductivity is one of the most important temperature-dependent properties determining device performance. The operating temperature effect the properties of the electrolytes (e.g. viscosity, thermal stability, solubility, and ionic conductivity). Thus, it leads to changes in capacitance and ESR with temperature. In our experiment, in order to compare the influence of the temperature on ESR and capacitance of propylene carbonate electrolyte, the device performance at room temperature (RT) was compared with measurements at low and high temperatures. The supercapacitor was subjected to a climatic test chamber (ESPEC). The results are presented and discussed in Section **3.5**. In addition, the viscosity of the electrolyte solution was measured at the temperature range between -10 °C and 70 °C using Anton Paar MCR301 rheometer and discussed in Section **3.4**.

Next, the robustness of the devices under bending was investigated. While commercial supercapacitors are mostly provided in rigid can-like packages, printed supercapacitors have the potential to be highly flexible, and thus easy to integrate into thin, flexible device applications. We have performed cyclic bending tests on our devices using a Mark 10 ESM303 test system and following the IPC-9204 guidelines on flexibility and stretchability testing for printed electronics. By applying very low force, the sample was reproducibly bent with radius of 0.41 cm, as determined by optical imaging. The setup used for the tests is shown in figure **7** (a,b,c). One end of the device was attached to the upper grip and the other end was attached to the lower grip. The lower

grip was fixed, and the upper grip was adjustable, moving up and down, thus bending the supercapacitors for a specified number of cycles, 8 secs/cycle. Cyclic voltammetry was used to characterize the electrical response of the supercapacitors during these mechanical deformations. The results are presented and discussed in Section **3.6**.

In our final experiments, the printed supercapacitors were subjected to thermal shock cycling in a dedicated climate chamber between temperature extremes of -40 °C and 100 °C. The temperature change rate between the extremes of temperatures was 90°/min and dwell time at each temperature extreme 15 minutes, resulting in an approximately 30-minute cycle. Altogether 500 cycles were conducted. The electrical parameters of the supercapacitors were measured before testing as well as after 100, 300, and 500 cycles. The thermal shock cycle of the process is shown in figure **9**, where the temperature is set to T_0= -40 °C and T_1 = 100 °C, t1=t2= 15 minutes. The results are discussed in Section **3.8**.

3. Results and discussion

3.1 Cyclic voltammetry measurement

CV is often used in electrochemical studies. Using equations (**1**,**2**) [33][34], the capacitance value was calculated. As indicated in figure **2**(a), CV sweeps were obtained at various scan rates ranging from 10 mVs^{-1} to 80 mVs^{-1} at voltage range from 0 to 2.5 V. Figure **2**(b) shows the measured capacitance value from 9 to 10 mF at different scan rates. The capacitance, voltage, and ESR of these devices are sufficient for a two-cell module to apply in BLE transmission.

The expression for the current with applied voltage V(t) to the supercapacitor is given as follow.

$$I(t) = C\frac{dV}{dt} \quad \text{---------- } \mathbf{1}$$

The capacitance relation with current and scan rate is given by

$$C = \frac{I(t)}{dV/dt} \quad \text{---------- } \mathbf{2}$$

where dV/dt is the scan rate.

The CV curves show symmetric rectangular shapes that are close to ideal capacitive behaviors of the cells. Figure **2**(c) shows device's galvanostatic charge-discharge curves with a constant current of 1 mA, 3 mA, and 10 mA from 0 to 2.5 V. The charging-discharging curves of the device are relatively symmetrical which good capacitive characteristics. Furthermore, voltage-time curves are linear, implying that the electrodes are stable [34][35].

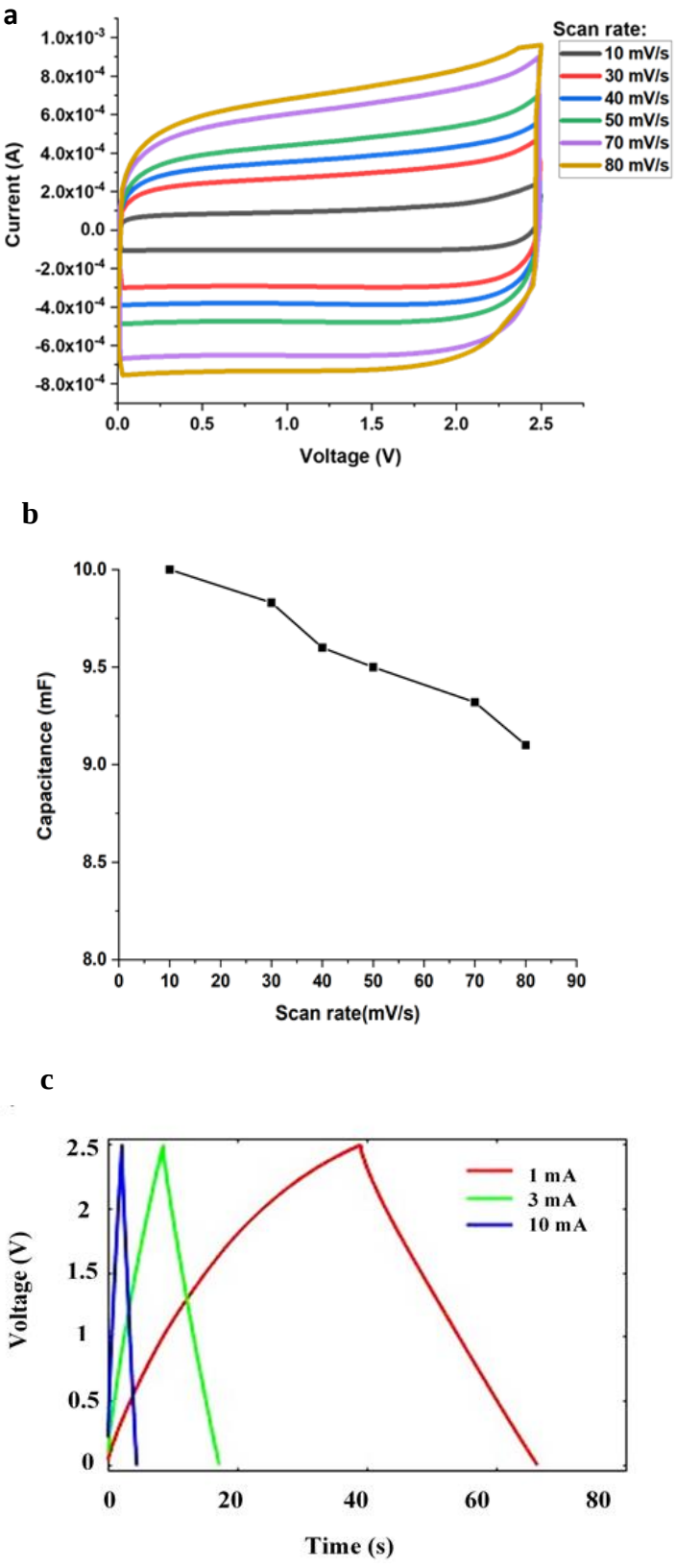

Figure 2. A plot of cyclic voltammetry measurement (a), capacitance vs scan rate (b), and charge-discharge measurement (c).

The specific capacitance was measured by dividing the capacitance value by total electrode mass. The electrode mass of the active materials was from 10.4 to 10.7 mg. The measured specific capacitance was from 0.76 to 0.93 Fg^{-1}. Similarly, the measured current per unit mass value was from 30.3 to 35.5 mAg^{-1} at scan rate 40 mVs^{-1}. The specific capacitance value is low, which consistent with the targeted capacitance below 10 mF. By comparison, the specific capacitance of devices comprising activated carbon electrodes has been reported to be between 16 to 26 Fg^{-1} [32].

3.2 Electrochemical impedance spectroscopy

This electrochemical method is often applied to characterize the supercapacitors. This method starts with applying an AC voltage to an electrochemical cell and then measuring current flowing through it. The amplitude of the excitation signal 10 mV with excitation frequency in the range from 1 Hz to 1 MHz. The Nyquist plot of the supercapacitor is shown in figure **3**(a). Figure **3**(b) shows plot of impedance (real and imaginary) as a function of frequency. As described in Equation (**3**), the total impedance (Z) is a combination of real and imaginary values. The equivalent series resistance is measured from real part of the Nyquist plot.

$$Z = \sqrt{Z''^2 + Z'^2} \quad \text{---------- } \mathbf{3}$$

Where, Z'' and Z' are imaginary and real part respectively.

The porous structure of the active material result a slope line of 45° at the intermediate frequency, which defines the distributed resistance and is also known as Warburg diffusion region. The steeper slope indicates higher diffusion capability of ions entering the pores [36]. At high frequencies ranging from 1 kHz to 1 MHz, a semi-circle loop was observed. As shown in figure **3**(a,b), the ESR intersects the real axis Z'and decreases towards higher frequencies. The ESR value of device was from 1.1 Ω to 2 Ω. The ESR consists of the electrolyte resistance (denoted as R_1, left most intersect Z'), electrode and current collector's contact resistance (denoted as R_2, width of the semicircle), and porous active material's distributed resistance (denoted as R_3, 45° segment) [9][32].

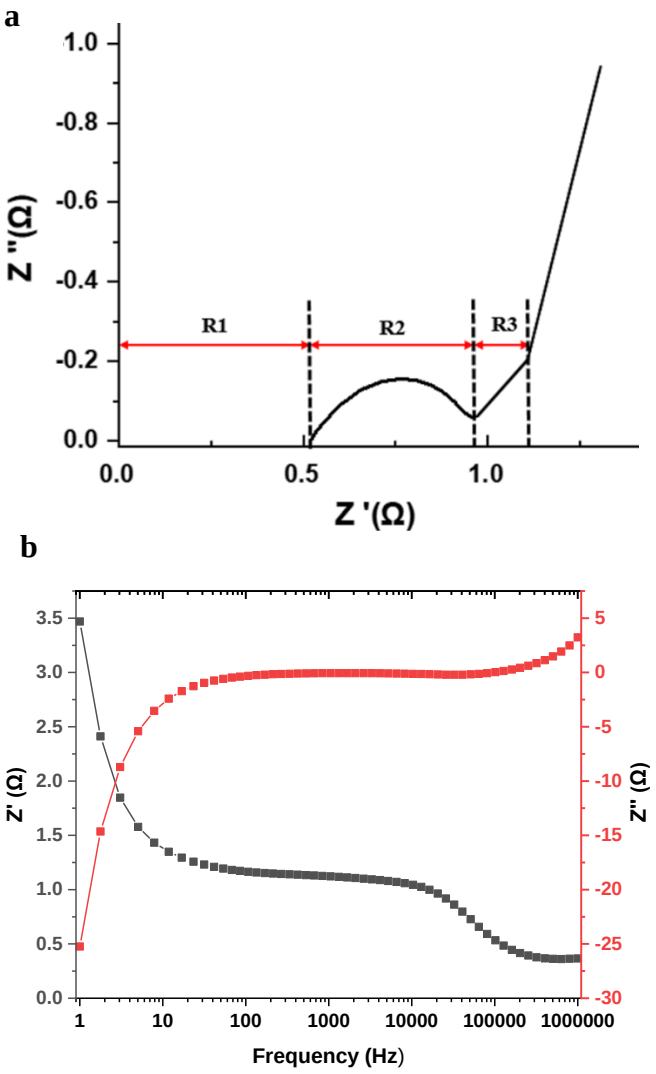

Figure 3. Nyquist plot (a), and plot of real and imaginary impedance as function of frequency (b)

3.3 Leakage current

The leakage current in our supercapacitors was measured by applying 2.5 V for 24 hours. Inorder to maintain that voltage level, a small float current needed which is called a leakage current. By using the industrial standard IEC 62391-1 [37], leakage current was recorded. Very low leakage current between 0.1 µA and 0.4 µA was measured. The impurities at the electrodes due to Faradiac charge-transfer reactions may cause small residual leakage current. The impurities which are frequently found in carbon materials may be transition metal ions. Final assembly of these devices in glove box and robust sealing is very important to prevent water or oxygen from entering the devices.

3.4 Ionic conductivity and viscosity

The ionic conductivity of the 1 M $TEABF_4$ in PC electrolyte was measured at room temperature by EIS. The expression for the ionic conductivity is by equation 4.

$$\sigma = \frac{l}{RA} \text{ ----------}\mathbf{4}$$

where σ is an ionic conductivity, l is distance between electrodes, R is the resistance of the electrolyte and A is the electrode surface area. The electrode surface area is about 10.5 cm^{-2} and separation distance between them was 1 mm. The ionic resistance measured from Nyquist plot was about 0.8 Ω. The measured ionic conductivity of electrolyte was about 12 $mScm^{-1}$ which is close to earlier publication [12][38].

Viscosity is defined as the ratio of the shear stress to the shear rate. The expression for the viscosity is by equation 5.

$$\eta = \frac{T}{\gamma} \text{ ----------}\mathbf{5}$$

where η is viscosity, T is shear stress and γ is a shear rate.

The plot of viscosity of an electrolyte as function of temperature is shown in figure 4. The viscosity shows temperature dependancy. The measured viscosity of the electrolyte at room temperature was 3.5 mPa s. This value is in between earlier reported data 2.5 mPa s [38][39] and 4 mPa s [40]. Similarly, the solubility and thermal behavior of the $TEABF_4$ in PC had been reported earlier [41][42][43].

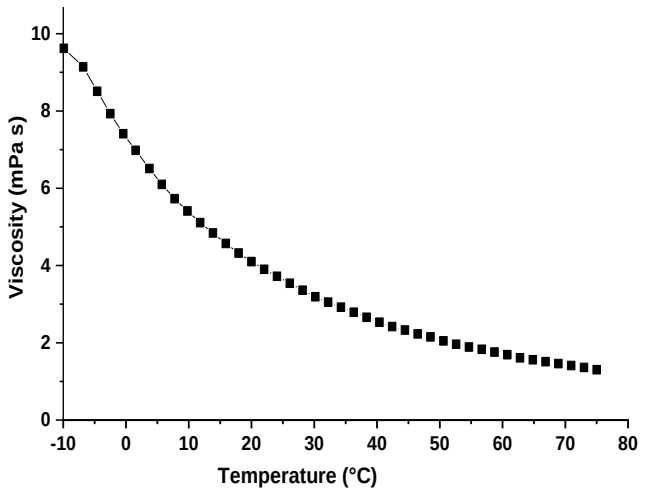

Figure 4. The plot of viscosity measurement of electrolyte as function of temperature between -10 °C to 70 °C .

3.5 Temperature test

The CV curves at scan rate 5 mVs^{-1} (0 - 2.5 V) and the EIS measurement graph, from which capacitance and ESR were determined between -40 °C and 100 °C, are shown in figure **5**(a,c**)**. The CV curves are relatively rectangular, indicating good capacitor performance and electrode stability. However, the area of the curve changes due to the effect of temperature on the electrochemical performance of the supercapacitor. The reference RT capacitance and ESR values were 8.5 mF and 1.97 Ω, respectively. The plot of ESR as function of temperature is shown in figure **5**(b). Table **1** shows the supercapacitor capacitance and ESR performance under different temperature conditions. The dependence of capacitance on temperature is substantially weaker than the dependence of ESR. The capacitance increased by 11% at 100 °C and decreased by 7 % at -40 °C. On the other hand, there is a significant change in ESR with a decrease in temperature. The ESR value increases from 1.97 Ω to 4.98 Ω from RT to -40 °C. The increase in ESR at low temperature is due to the increased viscosity and reduced ionic conductivity of the electrolyte. As can be seen from figure **5**(c) with the help of the Nyquist plot, the major component contributing to ESR is the electrolyte resistance (leftmost intersect of the real axis Z'), which gradually increases with decreasing temperature.

At RT the electrolyte resistance was 0.55 Ω, which increased to 2.32 Ω at -40 °C. This results from the increased viscosity, which inhibits free movement of ions in the electrolyte and through the porous separator and pores in the carbon electrode. The second dominant factor was the distributed resistance due to ion diffusion in the porous active material which was 0.1 Ω and 0.9 Ω at RT and -40 °C, respectively. The difference in ESR is very small at high temperature. In addition, the supercapacitor retained its room temperature capacitance when cooled from 100 °C and defrosted from -40 °C, indicating stability and repeatability of the device.

The results reported here for flexible supercapacitors are consistent with earlier work on organic electrolytes-based supercapacitors in other architectures. Liu *et al* [18] investigated a rise in ESR for PC-based supercapacitors from 16 mΩ to 77 mΩ for RT and -30 °C. Kötz *et al* [9] reported an increase in ESR by 200% from 2.5 mΩ to 7.5 mΩ, mainly dominated by the distributed resistance at the 45° region. Zhi *et al* [44] reported significant changes in ESR from 135 mΩ to 876 mΩ at 60 °C and -40 °C respectively.

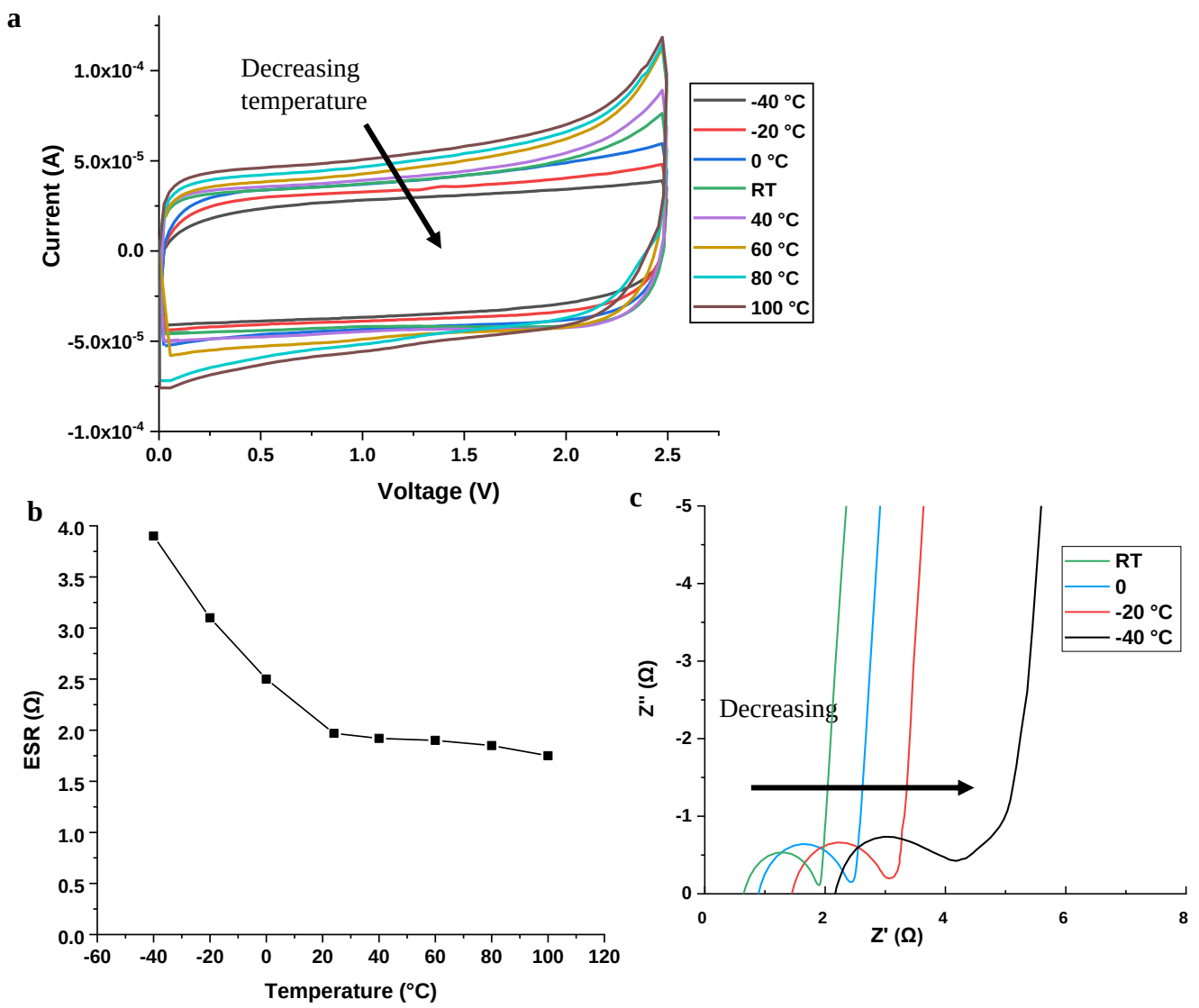

Figure 5. Cyclic voltammetry measurement at a different temperature from -40 °C to 100 °C at 5mV/s (a), Plot of equivalent series resistance vs temperature (b), and Nyquist plot of real and imaginary impedance (c)

Table 1. Capacitance and ESR change with temperature

Temperature (°C)	Capacitance (mF)	Change capacitance %	ESR	Change ESR %
100	9.5	11	1.78	-9.6
80	9.4	10.5	1.85	-6.0
60	9.3	9.4	1.9	-3.5
40	8.7	2.3	1.93	-2.0
RT	8.5	0	1.97	0
0	8.4	-1.1	2.5	26.9
-20	8	-5.8	3.13	58.8
-40	7.9	-7	4.98	153

The Coulombic efficiency (CE) of the device is defined as the ratio of total discharge capacity to the total charge capacity. The expression for the Coulombic efficiency is defined in equation 6.

$$CE(\%) = \frac{Q_{discharge}}{Q_{charge}} * 100 \text{----------} \mathbf{6}$$

where $Q_{discharge}$ and Q_{charge} are total charge storage capacities of the discharging and charging sweeps obtained from CV at scan rate of 5 mVs^{-1}. The CE value was between 93 % and 98.5 % when measured at temperatures from -40 °C to 100 °C. The CE value indicates good charge discharge behavior of the supercapacitors and is above 90 % even at sub-zero

temperatures. The plot of CE as function of temperature is shown in figure 6.

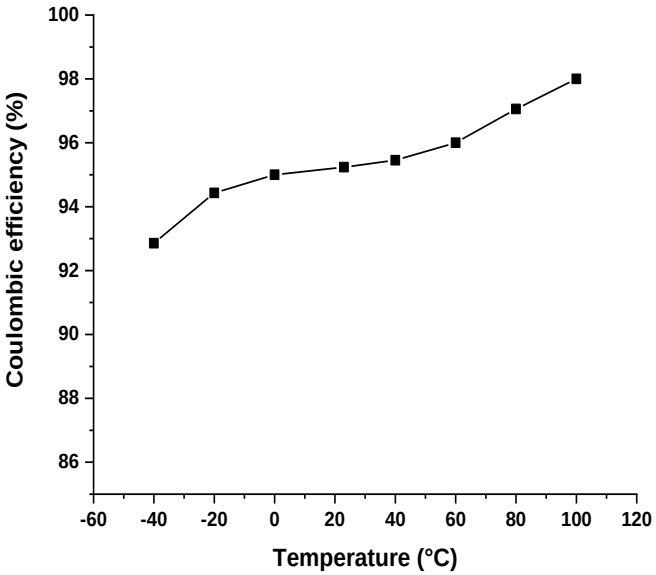

Figure 6: Coulombic efficiency at scan rate of 5 mVs^{-1} as a function of temperature.

3.6 Cyclic bending test

The cyclic voltammetry curves are almost identical, indicating excellent and long-term mechanical, electrical stability, and reliability under deformations. Figure **7** shows the Mark 10 measurement setup. Similarly, figure **8**(a) shows the CV measurement at up to 10000 bending cycles. The plot of capacitance retention is shown in figure **8**(b). We observed 100 % capacitance retention and the ESR was constant at about 1.1 Ω after 10000 bending cycles. The devices are well functional and the electrochemical performance is well maintained under various deformations. There was no sign of physical damage, delamination, or leakage in the device due to robust sealing. The minimum bending radius tested was 0.41 cm, which indicates sufficient flexibility for a wide range of printed and wearable electronics applications.

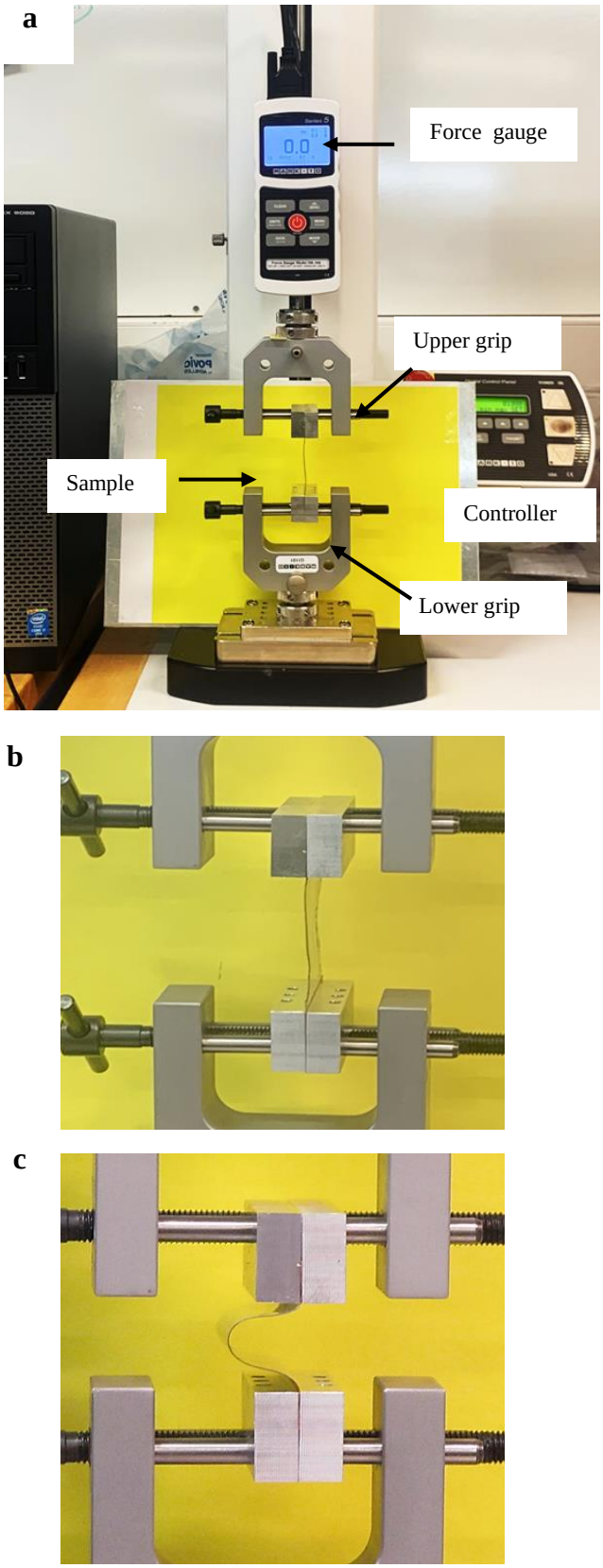

Figure 7: Photograph of mark 10 test setup system (a), before bend (b), after bend (c)

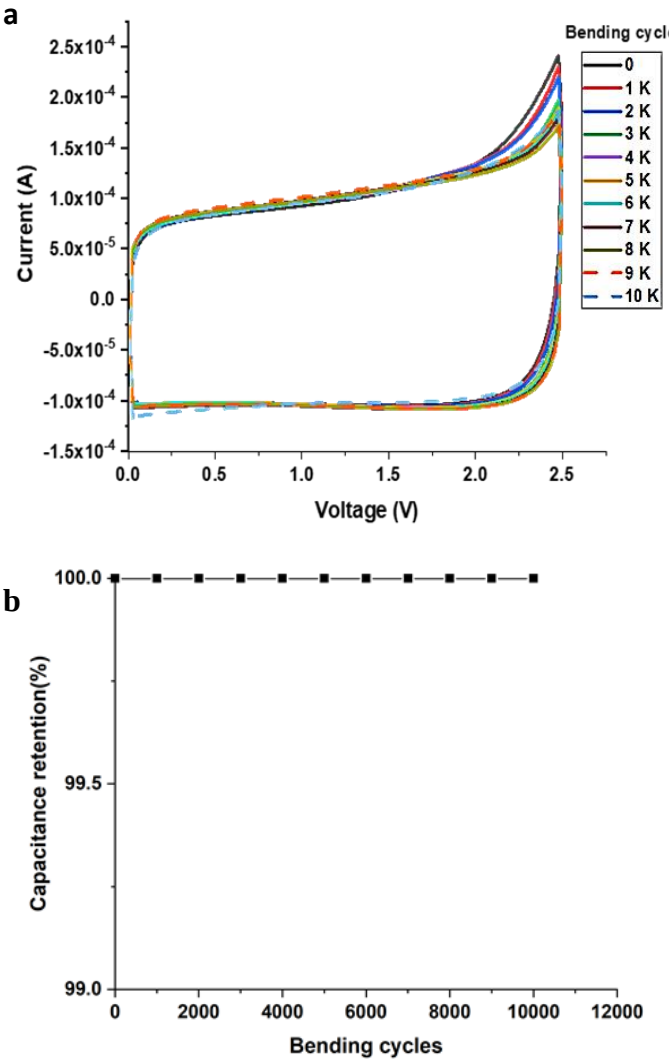

Figure 8. CV measurement up to 10000 bending cycles at scan rate 10mVs^{-1} (a), a plot of capacitance retention vs bending cycles (b)

3.7 Energy and power

The expression for the energy stored in the capacitor is given by equation 7 [45].

$$E = \frac{1}{2} CV^2 \quad \text{----------7}$$

where C is the capacitance and V is the voltage.

The energy storage capacity of the supercapacitor varies linearly with capacitance and quadratically with voltage. Thus, maximizing capacitance value and voltage will increase the energy [46]. The device capacitance value was between 8 and 10 mF and ESR in range 1.1 to 2 Ω. The maximum energy stored in supercapacitor was about 31.25 mJ. The energy density of supercapacitor can be defined relative to total electrode mass of active material. The measured maximum energy density was 3 J.g^{-1}. This energy density is lower than for activated carbon based supercapacitors, due to very low specific area of the carbon black electrode ink [8][47][48].

Similarly, the maximum power capability of the device is given by equation 8 [45].

$$P = \frac{V^2}{4R} \quad \text{----------8}$$

where R is the ESR and V is the voltage across the supercapacitor.

The power is inversely proportional to ESR, hence decreasing the ESR value and maximizing the electrolyte voltage will improve the power capability of the device. The calculated maximum power value was 1.42 W. The measured maximum power density was 133 W.g^{-1}.

3.8 Thermal shock test

Gualous et al [19] investigated the reaction of conventional supercapacitors to thermal shock and found a decrease in the electrical performance. However, in their study, the temperature was limited to between -20 °C to 80 °C and 20 cycles only, even though PC electrolyte has the potential to withstand temperatures much higher than 80 °C [20].

The area of the CV curves becomes smaller in size as shown in figure **10**(a), indicating reduced capacitance, and ESR increases as the number of test cycles increases. The supercapacitor behaves relatively well up to 100 cycles, followed by more severe degradation with increasing number of thermal shock cycles. The capacitance decreased to less than half of the initial value, from 9.5 to 3.5 mF, after 500 cycles. From the Nyquist plot of real and imaginary impedance, we observed that there is a significant increase in the contact resistance between the current collector and electrode at 500 cycles (width of semicircle), as shown in figure **10**(b). Even though the electrolyte and diffusion resistance increase, the contact resistance is dominant, at about 40 Ω. To investigate a possible cause, the electrodes were analyzed under a microscope Olympus BX51. As shown in figure **11**, the microscopic images show microstructural defects, cracks, and peel-off of the electrode after being subjected to thermal shock cycling. The degradation in the microstructure of the electrode layer results in weak contact with the current collector. This is believed to be due to the difference in coefficients of thermal expansion for the materials in the polymer/aluminum/carbon stack and is the most likely cause for the decrease in the electrical performance of the supercapacitors.

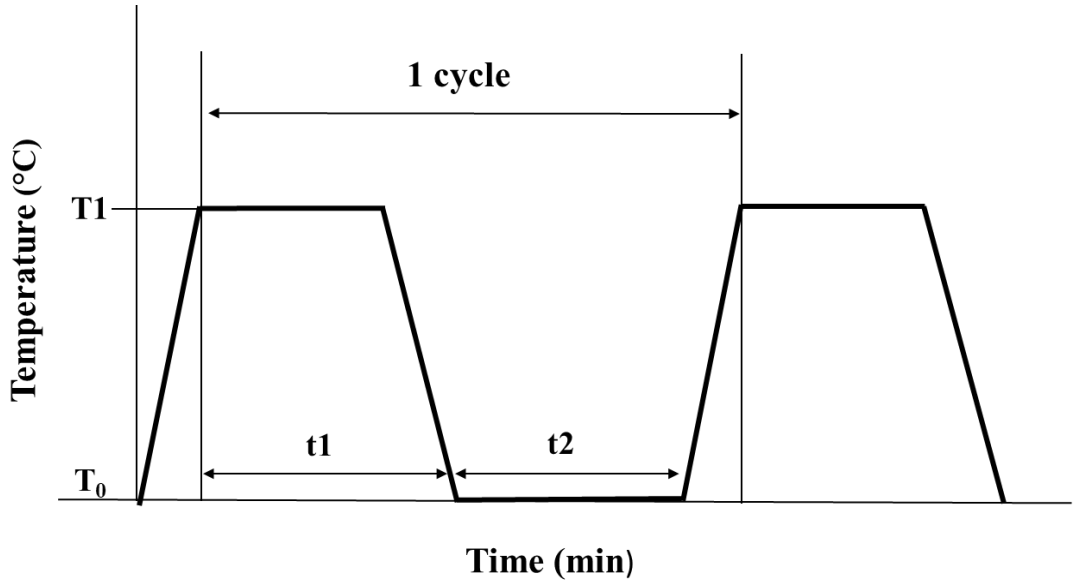

Figure 9. Thermal shock test process

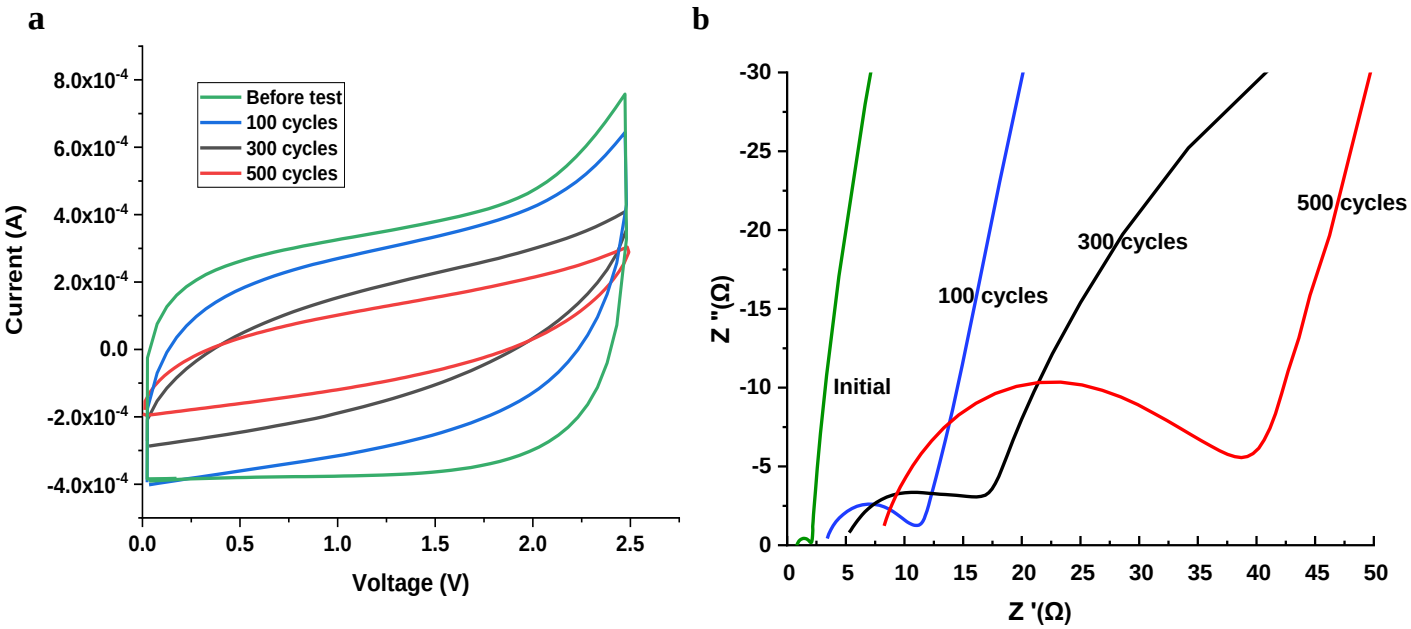

Figure 10. Cyclic voltammetry measurement at scan rate of 40mVs^{-1} before and after thermal shock test (a), and Nyquist plot (b) up to 500 cycles

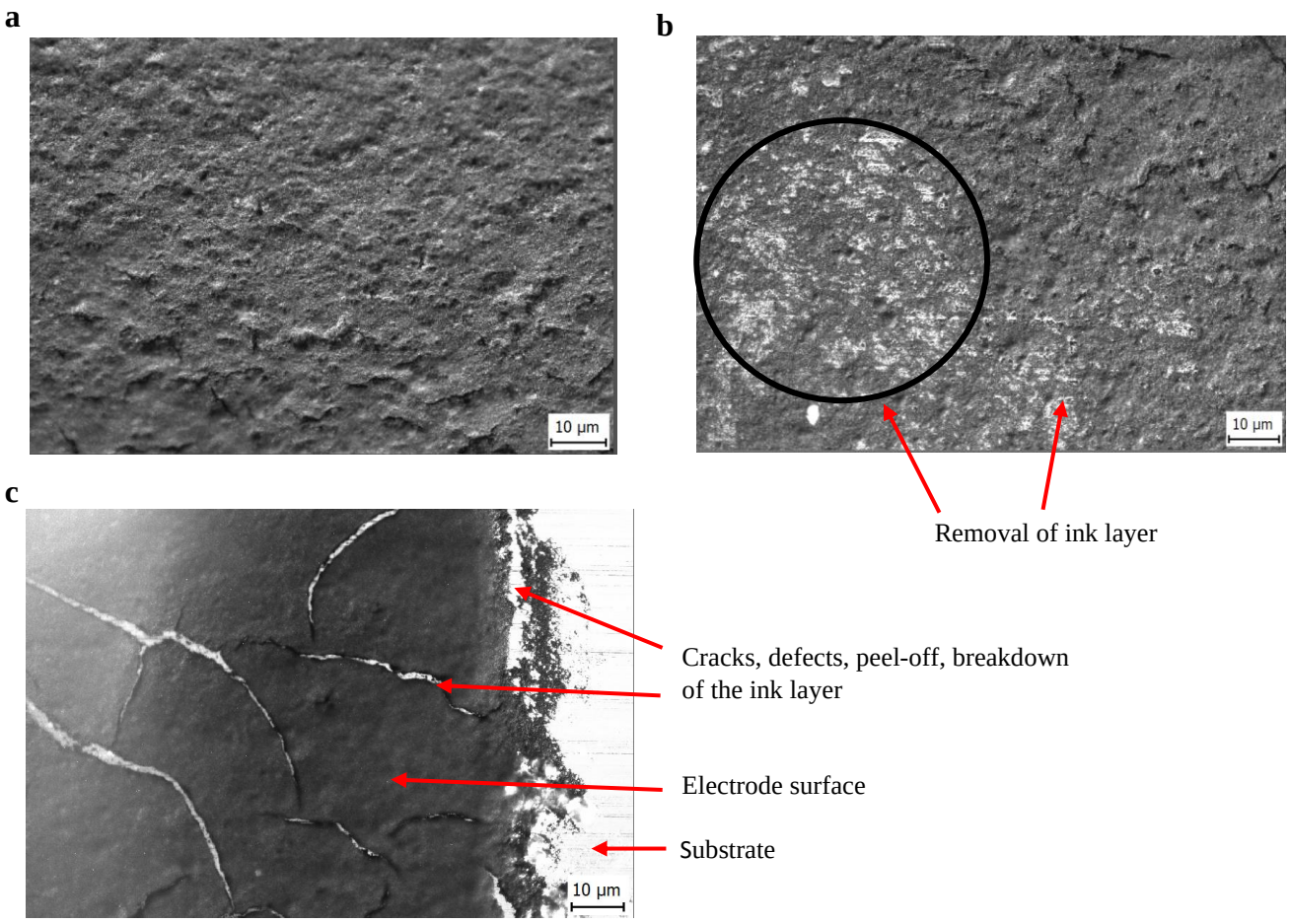

Figure 11: Microscopic images of printed electrode surfaces, before thermal shock test (a), and after thermal shock test (b**)** removal of the electrode layer (white spot area) and (c**)** cracks, defects, and peel off of the electrode layer

4. Conclusion

In this work, we report a systematic reliability study of an organic electrolyte-based, printable, and flexible supercapacitor. The devices, which contained 1 M $TEABF_4$/PC as electrolyte, were shown to operate successfully over the quite wide temperature range of -40 °C to 100 °C. The capacitance depends only weakly on temperature, while the ESR varies considerably. At sub-zero temperature, the ESR is the main limiting factor in terms of the electrical performance of the supercapacitor. Despite the stability to gradually changing temperature, thermal shock tests cause a significant decrease in device performance. This is due to an increase in contact as a result of formation of microcracks and defects in the porous electrode layer, which causes poor electrical contact to the current collector. The supercapacitors show excellent electrical performance under cyclic bending tests, confirming mechanical flexibility, stability, and robustness under up to 10000 bending cycles, with a minimum bending radius of 0.41 cm. Thus, these printed, simple structures, and lightweight supercapacitors are well suited and very promising for wearable and flexible electronics for energy storage applications.

Acknowledgements

This work was financially supported by the European Union's Horizon 2020 research and innovation programme under grant agreement no 825143, project Smart2Go. The infrastructure of Laboratory for Future Electronics at Tampere University is supported by Academy of Finland Finnish Research Infrastructure (FIRI, Grant No. 320019).

References

[1] Nyholm L, Nyström G, Mihranyan A and Strømme M 2011 Toward Flexible Polymer and Paper-Based Energy Storage Devices **23** 3751–69

[2] Keskinen J, Lehtimäki S, Dastpak A, Tuukkanen S, Flyktman T, Kraft T, Railanmaa A and Lupo D 2016 Architectural modifications for flexible supercapacitor performance optimization *Electron. Mater. Lett.* **12** 795–803

[3] Zhang R, Xu Y, Harrison D, Fyson J and Southee D 2016 A study of the electrochemical performance of strip supercapacitors under bending conditions *Int. J. Electrochem. Sci.* **11** 7922–33

[4] Wang S, Wei T and Qi Z 2009 Supercapacitor energy storage technology and its application in renewable energy power generation system *Proceedings of ISES World Congress 2007 (Vol. I -- Vol. V)* ed D Y Goswami and Y Zhao (Berlin, Heidelberg: Springer Berlin Heidelberg) pp 2805–9

[5] Krishnamoorthy K, Pazhamalai P, Mariappan V K, Manoharan S, Kesavan D and Kim S Two-dimensional Siloxene – graphene heterostructure-based high-performance supercapacitor for capturing regenerative braking energy in electric vehicles

[6] Moon H, Lee H, Kwon J, Suh Y D, Kim D K, Ha I, Yeo J, Hong S and Ko S H 2017 Ag/Au/Polypyrrole core-shell nanowire network for transparent, stretchable and flexible supercapacitor in wearable energy devices *Sci. Rep.* **7** 41981

[7] Keskinen J, Tuurala S, Sjödin M, Kiri K, Nyholm L, Flyktman T, Strømme M and Smolander M 2015 Asymmetric and symmetric supercapacitors based on polypyrrole and activated carbon electrodes *Synth. Met.* **203** 192–9

[8] Hung K, Masarapu C, Ko T and Wei B 2009 Wide-temperature range operation supercapacitors from nanostructured activated carbon fabric *J. Power Sources* **193** 944–9

[9] Kötz R, Hahn M and Gallay R 2006 Temperature behavior and impedance fundamentals of supercapacitors *J. Power Sources* **154** 550–5

[10] Dubal D P, Chodankar N R, Kim D H and Gomez-Romero P 2018 Towards flexible solid-state supercapacitors for smart and wearable electronics *Chem. Soc. Rev.* **47** 2065–129

[11] Nguyen H V T, Kim J and Lee K-K 2021 High-voltage and intrinsically safe supercapacitors based on a trimethyl phosphate electrolyte *J. Mater. Chem. A* 20725–36

[12] Zhong C, Deng Y, Hu W, Qiao J, Zhang L and Zhang J 2015 A review of electrolyte materials and compositions for electrochemical supercapacitors *Chem. Soc. Rev.* **44** 7484–539

[13] Shi S, Xu C, Yang C, Li J, Du H, Li B and Kang F 2013 Flexible supercapacitors *Particuologuy* **11** 371–7

[14] Liu S, Wei L and Wang H 2020 Review on reliability of supercapacitors in energy storage applications *Appl. Energy* **278** 115436

[15] Kim S K, Kim H J, Lee J C, Braun P V. and Park H S 2015 Extremely Durable, Flexible Supercapacitors with Greatly Improved Performance at High Temperatures *ACS Nano* **9** 8569–77

[16] Wang H, Liserre M, Blaabjerg F, Rimmen P, Jacobsen J B, Kvisgaard T and Landkildehus J 2014 Transitioning to physics-of-failure as a reliability driver in power electronics *IEEE J. Emerg. Sel. Top. Power Electron.* **2** 97–114

[17] Zhou D, Song Y, Liu Y and Blaabjerg F 2019 Mission profile based reliability evaluation of capacitor banks in wind power converters *IEEE Trans. Power Electron.* **34** 4665–77

[18] Liu P, Verbrugge M and Soukiazian S 2006 Influence of temperature and electrolyte on the performance of activated-carbon supercapacitors *J. Power Sources* **156** 712–8

[19] Gualous H, Gallay R, Alcicek G, Tala-ighil B, Oukaour A, Boudart B and Makany P 2010 Supercapacitor ageing at constant temperature and constant voltage and thermal shock *Microelectron. Reliab.* **50** 1783–8

[20] Jasinski R and Carroll S 1970 Thermal Stability of a Propylene Carbonate Electrolyte *J. Electrochem. Soc.* **117** 218

[21] Azaïs P, Duclaux L, Florian P, Massiot D, Lillo-Rodenas M A, Linares-Solano A, Peres J P, Jehoulet C and Béguin F 2007 Causes of supercapacitors ageing in organic electrolyte *J. Power Sources* **171** 1046–53

[22] Bittner A M, Zhu M, Yang Y, Waibel H F, Konuma

M, Starke U and Weber C J 2012 Ageing of electrochemical double layer capacitors *J. Power Sources* **203** 262–73

[23] Hahn M, Kötz R, Gallay R and Siggel A 2006 Pressure evolution in propylene carbonate based electrochemical double layer capacitors *Electrochim. Acta* **52** 1709–12

[24] Oz A, Gelman D, Goren E, Shomrat N, Baltianski S and Tsur Y 2017 A novel approach for supercapacitors degradation characterization *J. Power Sources* **355** 74–82

[25] Lu C and Chen X 2020 All-Temperature Flexible Supercapacitors Enabled by Antifreezing and Thermally Stable Hydrogel Electrolyte *Nano Lett.* **20** 1907–14

[26] Dai H, Zhang G, Rawach D, Fu C, Wang C, Liu X, Dubois M, Lai C and Sun S 2021 Polymer gel electrolytes for flexible supercapacitors: Recent progress, challenges, and perspectives *Energy Storage Mater.* **34** 320–55

[27] Sundriyal P and Bhattacharya S 2019 Scalable Micro-fabrication of Flexible, Solid-State, Inexpensive, and High-Performance Planar Micro-supercapacitors through Inkjet Printing *ACS Appl. Energy Mater.* **2** 1876–90

[28] Liu Y, Li H, Wang X, Lv T, Dong K, Chen Z, Yang Y, Cao S and Chen T 2021 Flexible supercapacitors with high capacitance retention at temperatures from -20 to 100 °c based on DMSO-doped polymer hydrogel electrolytes *J. Mater. Chem. A* **9** 12051–9

[29] Na Y W, Cheon J Y, Kim J H, Jung Y, Lee K, Park J S, Park J Y, Song K S, Lee S B, Kim T and Yang S J 2022 All-in-one flexible supercapacitor with ultrastable performance under extreme load *Sci. Adv.* **8** 1–11

[30] Rokaya C, Keskinen J and Lupo D 2022 Integration of fully printed and flexible organic electrolyte-based dual cell supercapacitor with energy supply platform for low power electronics *J. Energy Storage* **50** 1–10

[31] Keskinen J, Sivonen E, Jussila S, Bergelin M, Johansson M, Vaari A and Smolander M 2012 Printed supercapacitors on paperboard substrate *Electrochim. Acta* **85** 302–6

[32] Lehtimäki S, Railanmaa A, Keskinen J, Kujala M, Tuukkanen S and Lupo D 2017 Performance, stability and operation voltage optimization of screen-printed aqueous supercapacitors *Sci. Rep.* **7**

[33] Rokaya C, Keskinen J, Bromels C, Sch ffner P, Küzeci E and Lupo D 2021 Polymer-based printed electrolytic capacitor and its circuitry application in a low pass filtering, rectifying and energy storage unit *Flex. Print. Electron.* **6** 1–11

[34] Wang W, Yuan Y, Yang J, Meng L, Tang H, Zeng Y, Ye Z Z and Lu J 2018 Hierarchical core–shell Co3O4/graphene hybrid fibers: potential electrodes for supercapacitors *J. Mater. Sci.* **53** 6116–23

[35] Liu Y, Weng B, Razal J M, Xu Q, Zhao C, Hou Y, Seyedin S, Jalili R, Wallace G G and Chen J 2015 High-performance flexible all-solid-state supercapacitor from large free-standing graphene-PEDOT/PSS Films *Sci. Rep.* **5** 17045

[36] Awitdrus A, Suleman M, Syahirah N and Shamsudin S 2016 Energy and power of supercapacitor using carbon electrode deposited with nanoparticles nickel oxide *Int. J. Electrochem. Sci.* **11** 95–110

[37] IEC 62391-1 2006 *International standard : Fixed electric double-layers capacitors for use in electronic equipment-Part 1: Generic Specification* (Geneva)

[38] Brandt A, Castro C, Anouti M and Balducci A 2013 Journal of Materials Chemisty *An Investig. about use Mix. sulfonium-based Ion. Liq. Propyl. carbonate as electrolytes supercapacitors* **1** 12669–78

[39] Chen W, Rakhi R and Alshareef H 2012 High energy density supercapacitors using macroporous kitchen sponges *J. Mater. Chem.* **22** 14394–402

[40] Sillars F, Fletcher I, Mirzaeian M and Hall P 2012 Variation of electrochemical capacitor performance with room temperature ionic liquid electrolyte viscosity and ion size *Phys. Chem. Chem. Phys.* **14** 6094–100

[41] Mikoto E 2007 Chemical capacitors and quaternary ammonium salts *J-stage Electrochem.* **75** 565–71

[42] KOEI Ionic liquids for electrolytes

[43] Tyunina E, Afanas'ev V and Chekunova M 2012 Viscosity and density of solutions of tetraethylammonium tetrafluoroborate in propylene carbonate at different temperatures *J. Solution Chem.* **41** 307–17

[44] Zhang Z, Lai Y, Li J and Liu Y 2009 Electrochemical behavior of wound supercapacitors with propylene carbonate and acetonitrile based nonaqueous electrolytes *J. Cent. South Univ. Technol.* **16** 247–52

[45] Kötz R and Carlen M 2000 Principles and applications of electrochemical capacitors *Electrochim. Acta* **45** 2483–98

[46] Keskinen J 2018 *Supercapacitors on Flexible*

Substrates for Energy Autonomous Electronics (Tampere: Tampere University)

[47] Keskinen J, Railanmaa A and Lupo D 2018 Monolithically prepared aqueous supercapacitors *J. Energy Storage* **16** 243–9

[48] Sun X, Zhang X, Zhang H, Huang B and Ma Y 2013 Application of a novel binder for activated carbon-based electrical double layer capacitors with nonaqueous electrolytes *J. Solid State Electrochem.* **17** 2035–42